Mon. Not. R. Astron. Soc. **000**, 000–000 (2003)

# Top-Down Fragmentation of a Warm Dark Matter Filament

Alexander Knebe[1], Julien E. G. Devriendt[2], Brad K. Gibson[1], Joseph Silk[2]
[1] *Centre for Astrophysics & Supercomputing, Swinburne University, P.O. Box 218, Mail # 31, Hawthorn, Victoria, 3122, Australia*
[2] *Astrophysics, Oxford University, Keble Road, Oxford, OX1 3RH, UK*

Received ...; accepted ...

**ABSTRACT**
We present the first high-resolution $N$-body simulations of the fragmentation of dark matter filaments. Such fragmentation occurs in top-down scenarios of structure formation, when the dark matter is warm instead of cold. In a previous paper (Knebe et al. 2002, hereafter Paper I), we showed that WDM differs from the standard Cold Dark Matter (CDM) mainly in the formation history and large-scale distribution of low-mass haloes, which form later and tend to be more clustered in WDM than in CDM universes, tracing more closely the filamentary structures of the cosmic web. Therefore, we focus our computational effort in this paper on *one* particular filament extracted from a WDM cosmological simulation and compare in detail its evolution to that of the same CDM filament. We find that the mass distribution of the halos forming via fragmentation within the filament is broadly peaked around a Jeans mass of a few $10^9$ $M_\odot$, corresponding to a gravitational instability of smooth regions with an overdensity contrast around 10 at these redshifts. Our results confirm that WDM filaments fragment and form gravitationally bound haloes in a top-down fashion, whereas CDM filaments are built bottom-up, thus demonstrating the impact of the nature of the dark matter on dwarf galaxy properties.

**Key words:** cosmology – dark matter – numerical simulations

## 1 INTRODUCTION

The Cold Dark Matter crisis on small scales is far from being resolved. First, the highest resolution simulations available still favour "cuspy" galaxy haloes (Power et al. 2003) with an inner slope for the density profile $\approx -1.2$, whereas high resolution observations of low surface brightness galaxies are best fit by halo "cores" (de Block & Bosma 2002; Swaters et al. 2003). Second, the dearth of low luminosity galaxy satellites found $N$-body simulations remains, although squelching of dwarfs due to the reionisation of the universe at high redshift may provide a solution (e.g. Benson et al. 2002; Somerville 2002). However, it is unclear that such a process is the definite solution, because the low-mass dark satellite haloes left over still interact gravitationally with the luminous galaxies, exchanging energy and angular momentum with them. Such interactions could have a significant impact on these galaxies' properties, heating their disks and reducing their sizes. Direct observational probing of dark matter halo substructure through anomalies in the flux ratio of multiple-image quasar lenses could in principle determine whether the scenario previously suggested is the correct one (Metcalf & Madau 2001; Dalal & Kochanek 2002), but there still are major difficulties to overcome in order to obtain reliable estimates of the amount of mass locked in dark substructures (Chen et al. 2003).

An alternate mechanism to solve the satellite problem, which does not suffer from these side effects, is to reduce the power of dark matter fluctuations on small scales. This can be accomplished by changing the nature of the dark matter, (e.g. Kaplinghat, Knox, & Turner 2000; Spergel & Steinhardt 2000; Colin et al. 2000; Bode, Ostriker & Turok 2001; Avila-Reese et al. 2001), by advocating an inflationary model with broken-scale invariance (Kamionkowski & Liddle 2000) or by simply assuming an "unusual" dip in the primordial CDM power spectrum on small scales (Little, Knebe & Islam 2003). The latest constraints from polarisation measurements of the Cosmic Microwave Background Radiation by WMAP (Bennett et al., 2003; Spergel et al., 2003; Kogut et al., 2003) seem to exclude such models, with the major caveat that the current theoretical understanding of the objects that produce the first ionising photons is at best crude. As an example, a reionisation redshift of 11 (on the lowest side of the WMAP published 95 % confidence level) is still reached in a WDM model for which the warmon mass is about 1 keV, provided the objects responsible for photoionising the universe at this redshift emit on average between 100 and 1000 times more ionising photons per baryon than

normal stars, as is possible with a top–heavy IMF dominated by accreting black holes (Schneider et al. 2002). Moreover, the constraints become less restrictive as the mass of the warmon increases.

More sophisticated numerical simulations of high-redshift WDM–like universes, combined with a better understanding of the reionising photon emitters are required in order to set definitive constraints on the nature of the dark matter from polarization measurements. This important point set aside, previous simulations (see Paper I; Bode, Ostriker & Turok 2001; Avila-Reese et al. 2001) have indicated that deviation of WDM models from the CDM hierarchical structure formation scenario should be more pronounced in low density regions (e.g. filaments, voids). More specifically, in these simulations, most of the halos close to the resolution limit (i.e. less than 100 particles) seemed to be forming at smaller redshifts than in the standard CDM models, and in a top-down fashion through the break-up of filamentary structures. This phenomenon is of prime interest for galaxy formation and evolution models as it predicts that dwarfs properties strongly depend on the nature of the dark matter. It also gives rise to a series of interesting questions: how much do filaments fragment? When do they fragment the most? What is the mass distribution of the fragments? To tackle this issue we identified one of the filaments in the previous CDM and WDM low resolution runs presented in Paper I and resimulated it with a mass resolution 64 times higher than the original.

This paper proceeds as follows: in Section 2 we briefly give the model parameters and describe the $N$-body-simulations which we use in Section 3 to calculate the properties of gravitationally bound halos found in the filament and of the filament itself. Finally, we present our conclusions in Section 4.

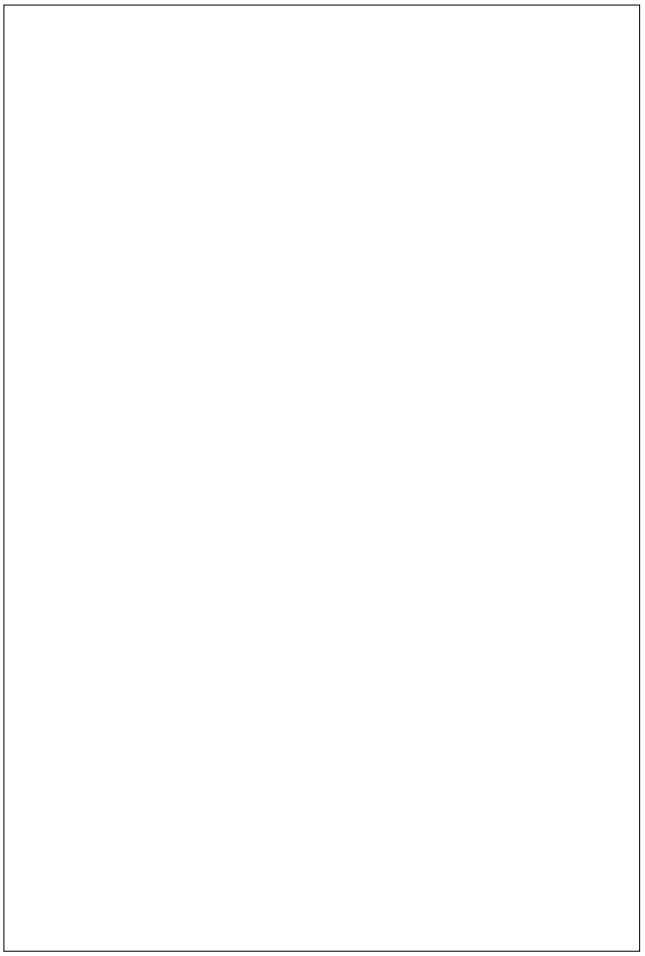

**Figure 1.** Gray-scaled image of the logarithm of the density field around the filament at redshifts $z = 1$ (upper panel), $z = 3$ (middle panel) and $z = 5$ (lower panel).

## 2 $N$-BODY SIMULATIONS

The ΛWDM and the ΛCDM cosmological parameters used in this paper are the same as those of the ΛWDM2 and ΛCDM runs presented in Paper I, namely, $\Omega_0 = 1/3$, $\lambda_0 = 2/3$, $\sigma_8 = 0.88$, $h = 2/3$, and $m_{\rm WDM} = 0.5$keV. We note that they are in good agreement with the latest results from WMAP (Bennett et al. 2003).

As outlined in Paper I, initial conditions for our lower resolution simulations were generated by packing particles from higher resolution initial conditions into groups. For the simulations presented in this paper, we simply identified a filament at $z = 0$ in our 25 $h^{-1}$ Mpc low resolution box, tracked back in time the Lagrangian volume its particles occupied at $z = 35$, and unpacked the low-resolution particles into high-resolution particles in that region. In practice, our resimulation of the filament resulted in a 64-fold increase in mass resolution from $m_p \simeq 7 \times 10^8 h^{-1}$ M$_\odot$ ($128^3$ particles) in the low resolution runs to $m_p \simeq 10^7 h^{-1}$ M$_\odot$ ($512^3$ particles) in the runs presented here. Each of our ΛWDM and ΛCDM filaments contains over 3 million high resolution particles and our force resolution is of the order 3 $h^{-1}$ kpc in the densest regions. The total length of a filament can be represented by the dimensions $x_b = 7$, $y_b = 4$, $z_b = 6$ (in $h^{-1}$ Mpc) of the rectangular box enclosing it. We took "snapshots" of the simulations at the following redshifts: $z$=5, 4.5, 4, 3.5, 3, 2.5, 2, 1.75, 1.5, 1.25, 1, 0.5, and 0. These re-simulations were undertaken using the publicly available Adaptive Mesh Refinement code `MLAPM` (Knebe, Green & Binney, 2001).

Particle groups were identified using the Bound Density Maxima (BDM, Klypin & Holtzman 1997) method, in keeping with Paper I. The BDM code identifies local overdensity peaks by smoothing the density field on a particular scale of the order of the force resolution. We adopted a smoothing of $10h^{-1}$ kpc for the runs under investigation. These peaks are prospective halo centres. For each of these halo centres we step out in (logarithmically spaced) radial bins until the density reaches $\rho_{\rm halo}(r_{\rm vir}) = \Delta_{\rm vir}\rho_b$, where $\rho_b$ is the background density and $\Delta_{\rm vir} \approx 340$. This defines the outer radius $r_{\rm vir}$ of the halo. Once we know the outer radius we are able to calculate internal properties of the halos. Note that during this group identification procedure we also check if each individual particle truly belongs to the halo by comparing its velocity to the local value of the escape velocity. We exclude unbound particles from the haloes. This iterative method ensures that we only retain gravitationally bound objects.

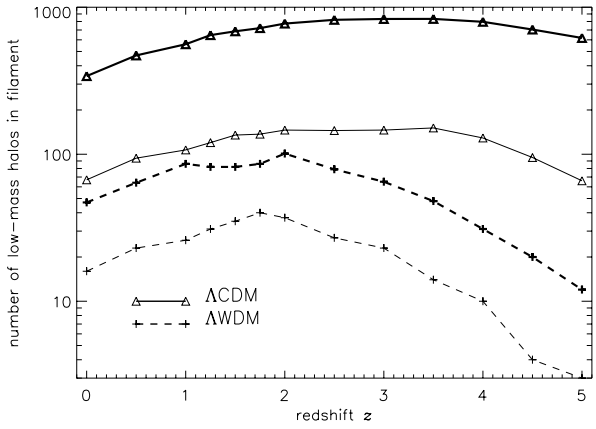


**Figure 2.** Number of gravitationally bound halos located with the filament as a function of redshift. We employed a mass cut of $M > 10^9 h^{-1}$ M$_\odot$ (thick lines) and $M > 10^{10} h^{-1}$ M$_\odot$ (thin lines), respectively.

## 3 RESULTS

### 3.1 Dark Matter Density Field

We begin our investigation by looking at the large-scale structure density field within and around the filament. Fig. 1 shows the particle distribution for both models with each particle being grey-scaled proportionally to the logarithm of the local (over-)density. A striking feature of Fig. 1 is the marked granularity of the density field in the CDM model at all redshifts in contrast with WDM. This effect reflects the lack of filtering of power on small scales in CDM as opposed to WDM. However, while the WDM filament is obviously different from its CDM counterpart at redshift $z$=5, they are very similar at $z$=1. This similarity is all the more remarkable that the logarithmic scale used to plot the density fields shown in Fig. 1 artificially enhances the density contrast, thus highlighting differences between the two universes that would have gone unnoticed had the scale been linear.

A further difference of note is the *appearance* of individual (low-mass) halos during the course of the WDM filament evolution, whereas dense objects only seem to be merging in the CDM filament, therefore *decreasing* steadily in number.

We have not presented results at redshift $z = 0$ because the picture at this epoch is qualitatively similar to that at reshift $z = 1$: most of the interesting processes leading to different looking WDM and CDM filaments occur at high redshifts ($z > 1$).

### 3.2 Halo Abundance in the Filament

To quantify the discussion in Section 3.1, we compute how the number of halos within the filament evolves with redshift. This number is plotted in Fig. 2, and contains all gravitationally bound particle groups above $M > 10^9 h^{-1}$ M$_\odot$ (more than 100 particles – thick lines) and $M > 10^{10} h^{-1}$ M$_\odot$ (more than 1000 particles – thin lines), respectively. The former simply corresponds to the integral

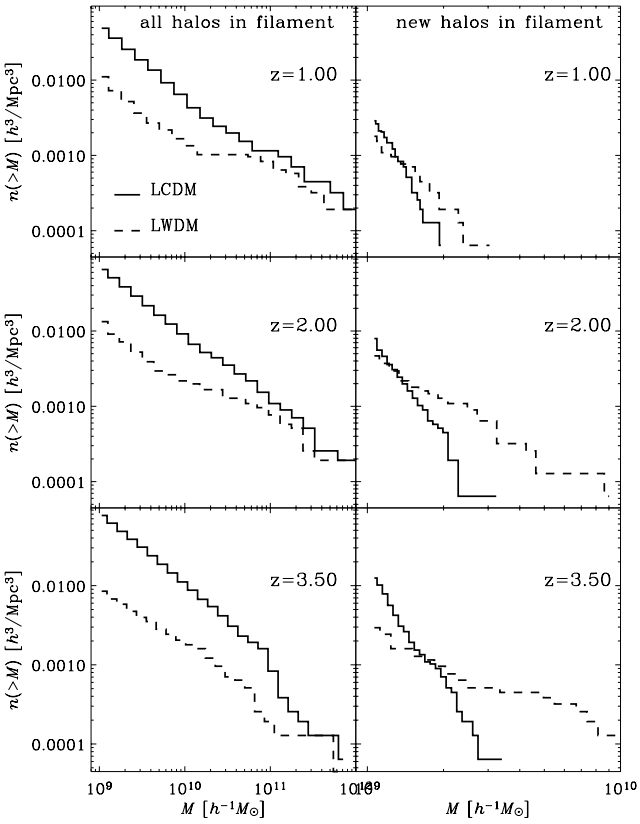


**Figure 3.** Cumulative mass functions of all halos located within the filament (left panel) along with the mass function of 'new' halos as defined in the text (right panel).

of the mass function over the entire halo mass range available given our resolution.

Fig. 2 demonstrates that independent of redshift, there are more halos in the CDM filament (as already expected from Fig. 1) than in the WDM filament. However, the ratio $N_{\rm halo}^{\rm CDM}/N_{\rm halo}^{\rm WDM}$, which appears to be nearly independent of the mass cut employed, drops significantly from about 50 at $z = 5$ to approximately 7 at $z = 2$. This ratio is a factor two smaller for the higher mass-cut of $10^{10} h^{-1}$ M$_\odot$. The depletion of halos in both models from $z = 2$ to $z = 0$ is readily explained when we consider that very few objects are created within the filament at low redshifts (see Fig. 5), and therefore, mergers must be the dominant process in determining the number of halos in that redshift range. Indeed, as can be seen in Fig. 1 haloes stream along the web-like structures to eventually become subsumed within larger objects (galaxy groups or clusters) located at the intersections of the filamentary network.

Fig. 3 displays the cumulative mass function of all halos identified within the filament (left panel) along with the mass function of 'new' halos (right panel). The definition of a 'new' halo is given in Section 3.4 where Fig. 3 is analysed in more detail, but for the moment one can simply view them as haloes which did not have any progenitor at the previous output. At this point of the analysis, we stress that the cumulative mass function of *all* halos in the CDM filament closely follows a power-law (with a slope close to -1)

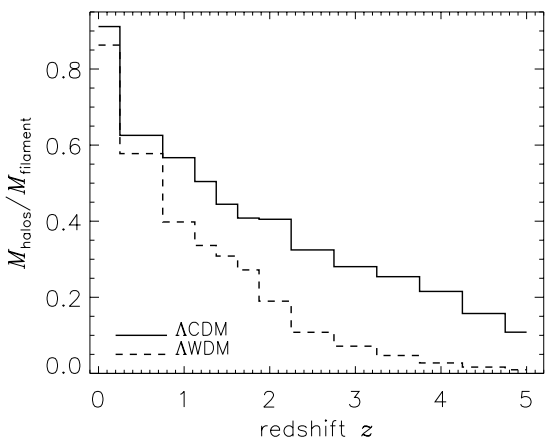


**Figure 4.** Fraction of mass within gravitationally bound halos of mass $M > 10^9 h^{-1}$ M$_\odot$ as a function of redshift.

whereas in the WDM case one observes a deficit of low-mass objects, in agreement with the results presented in Paper I.

### 3.3 Mass of the Filament

We next addres the question of the fraction of the filament material which gets locked up in galactic halos and how much remains smoothly distributed in the filament. To answer this question, we calculate the ratio of particles belonging to halos with $M > 10^9 h^{-1}$ M$_\odot$ (identified using the BDM code, cf. Fig. 2) to the total number of particles in the filament. This requires a definition for the boundary of the filament which follows from a previous definition for voids: Einasto et al. (1998) define *void particles* as having $\rho_p < \rho_b$ where $\rho_p$ is the local density at the particle position and $\rho_b$ the cosmological background density. We adopt the same prescription and call those particles that follow $\rho_p > \rho_b$ *filament particles*. The density at the particle position is interpolated from the density field calculated on a regular $256^3$ grid; as we restrict ourselves to only high-resolution particles we are at all times confined to the filament region (by definition).

The results of this analysis are plotted in Fig. 4. This figure highlights the overabundance of filament halos in CDM with respect to WDM, as the fraction of material in particle groups is at all times higher in the former than in the latter. Only at $z \lesssim 1$ does the ratio $M_{\rm halos}/M_{\rm filament}$ become comparable in both models, which confirms the similarity of these structures previously noticed at $z = 1$ (cf. Fig. 1). We note however that from Fig. 1 alone, one might have claimed that most of the material should already be in haloes at $z = 5$ in the CDM filament, but Fig. 4 argues against it, as only about 10 % of the particles belong to haloes more massive than $M > 10^9 h^{-1}$ M$_\odot$, for this model, at this redshift. Of course, in the CDM case, this percentage is quite sensitive to the mass cut-off adopted, in the sense that if we had chosen to consider haloes composed of 50 particles or more, it would have increased to about 20 %. Nevertheless, this implies that the gravitational field within the filament is still dominated by the smoothly distributed dark matter component up to redshifts $z \simeq 1$, both for the CDM and WDM filaments, and that accretion and merging are indeed important since the total number of halos decreases below $z = 2$ in both structures whereas the mass of each filament which is locked up within those haloes increases.

### 3.4 New Halos in the Filament

This leads us to the fundamental question of this study, namely *how* and *when* does the WDM filament fragment to form haloes? In other words, how important is this "top-down" fashion of forming haloes compared to the more traditional hierarchical "bottom-up" scenarios of CDM-like models? To tackle this issue, we constructed the merger tree of each individual halo between consecutive redshift outputs and tagged a halo as 'new' at a given redshift when no progenitor could be found at the previous output. The requirement for a progenitor to be identified as such was that it had to contain a minimum of 100 particles or 1/10 of the actual halo particles depending on which of these two numbers was the smallest. If such a progenitor was found the halo was marked 'old'. Fig. 5 shows the fraction of 'new' halos formed per unit time as a function of redshift. As can be seen from this figure, the interesting redshift range for this analysis is from $z = 4.5$ to $z = 2$, as one observes a significant halo formation rate within the WDM filament during this time period (cf. Fig. 5).

In order to obtain results not affected by spurious formation or evaporation of haloes between timesteps, we have set a lower mass limit of $10^9 h^{-1}$ M$_\odot$ (which translates into 100 particles). This means that if a halo is less massive than this cut-off it has been neglected in our analysis. However, this does not imply that its progenitor(s) had to contain 100 particles. The mass limit for the progenitor(s) is the minimum of 100 and 1/10 of the actual halo particles and hence can be as low as 10 particles (minimal mass for which a bound object can reasonably be detected). We emphasize that in the extreme case where a 10 particle progenitor of a halo is identified, it only affects the 'tag' of the halo currently under consideration, meaning that it is classified as 'old' instead of 'new'. More specifically, if such a progenitor turns out to be unphysical (a mere collection of 10 particles which happen to pass by one another quite slowly) it biases the results towards *fewer* new halos being created in the filament. In this sense, the curves plotted in Fig. 5 are lower limits on the true number of new haloes in the mass range $10^9 h^{-1}$ M$_\odot$ and above, as we have made sure that the halos marked as 'new' were not a part of *any* structure at the previous redshift. *Fig. 5 alone strongly suggests that the bulk of the halo population is forming between* $z = 4.5$ *and* $z = 2.5$ *within the WDM filament whereas the same figure points at the majority of halos being already in place in the CDM structure by* $z = 4$. To be more explicit, this figure shows that the WDM halo formation rate at $z = 3$ is still high enough that it could account for all halos present at this redshift, had it been constant in the past. But we also know from Fig. 2 that the maximum number of WDM halos is broadly peaked around $z = 2$, and from Fig. 5 that the halo formation rate is not constant but steeply increasing with redshift for $z > 2$. Furthermore, Fig. 5 and Fig. 7 tell us that the halo merger rate is negligible compared to the

**Table 1.** Characteristics of the 749 particles that end up forming the gravitationally bound halo at $z = 2$ shown in Fig. 6.

| redshift | $\langle\rho\rangle/\rho_b$ | $\langle r\rangle/(h^{-1}$ kpc) | $\Delta_{\rm vir}$ |
|---|---|---|---|
| $z = 2.0$ | 278 | 35 | 210 |
| $z = 2.5$ | 200 | 96 | 208 |
| $z = 3.0$ | 190 | 137 | 207 |
| $z = 3.5$ | 82 | 165 | 207 |

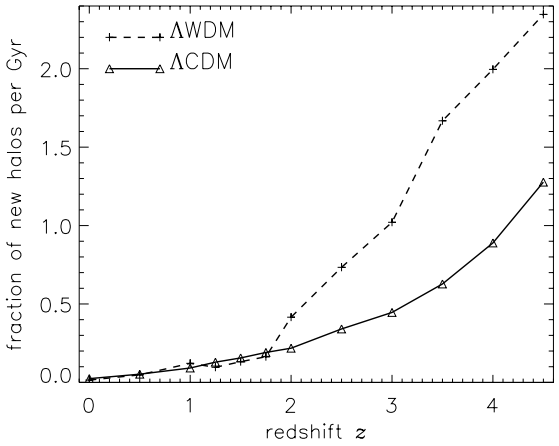


**Figure 5.** Fraction of halos per Gyr appearing in the filaments and for which no progenitor could be found at the previous redshift (new haloes). Note that the fraction becomes greater than unity at high redshift. This simply means that had the actual halo formation rate been the same at earlier times, more halos would have been formed than are currently present in the filament.

halo formation rate at $z \geq 2$. Therefore, we are forced to conclude that most halos were indeed 'born' in the WDM filament between $z = 5$ and $z = 2$. The same analysis, applied to the CDM filament leads to the claim that most halos are in place before $z = 5$.

This answers the question as to *when* the halos form out of the WDM filament, but Fig. 6 shows an example of *how* such a fragmentation occurs. The sequence of panels in that figure traces back in time all the particles found in a typical new halo of mass $M \approx 7.5 \times 10^9 h^{-1}$ M$_\odot$ at redshift $z = 2$ (i.e. a halo which was identified to be a 'new' gravitationally bound object at this redshift using the BDM algorithm). It is obvious from Fig. 6 that particles which end up within the virial radius of this halo at $z = 2$ are part of the filamentary structure until the very moment when the collapse takes place. The quantitative information obtained by tracing the particles pertaining to the final bound halo back in time and provided in Table 1 backs up this qualitative analysis. In particular, we computed in Table 1 the averaged local density (in terms of the background density) at all 749 particle positions, as well as the mean extent of the region occupied by those particles. As a reference we also listed the virial overdensity value $\Delta_{\rm vir}$ for each of the redshifts under consideration in the last column of Table 1.

To obtain a physical explanation for the fragmentation, we can calculate how the Jeans mass, $M_J$, varies with redshift in the WDM filament prior to its fragmentation, as-

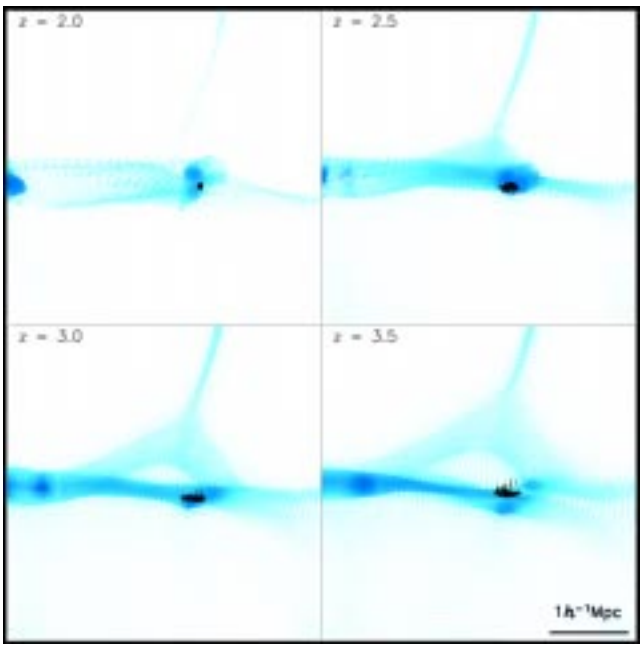


**Figure 6.** Example of a halo fragmentation within the WDM filament. All 749 particles which end up in the virial radius of the bound halo at $z = 2$ are shown in black. The grey-shaded area represents the density field within a filament slice. The thickness of this slice is equal to the maximal distance between halo particles at any time.

suming its density field to be close to homogeneous on scales larger than the Jeans scale $\lambda_J$. These masses and scales are given by the following formulae (e.g. Binney & Tremaine 1987):

$$M_J = \frac{\pi^{5/2}}{6G^{3/2}} \frac{\sigma_v^3}{\sqrt{(1+\delta)\rho_b}} \tag{1}$$

$$\lambda_J = \sqrt{\frac{\pi}{G\rho_b(1+\delta)}}\sigma_v \tag{2}$$

where $\rho \equiv (1+\delta)\rho_b$ is the density of the filament and $\sigma_v$ its averaged velocity dispersion. In the previous equations, $\delta$ stands for the (over-)density contrast within the filament with respect to the mean density of the background universe, $\rho_b$, at a given redshift. For our cosmological model, Eq. (1) and Eq. (2) become

$$M_J = 5.1 \times 10^7 (1+z)^{-3/2}(1+\delta)^{-1/2} \left(\frac{\sigma_v}{\rm km/s}\right)^3 {\rm M}_\odot \tag{3}$$

$$\lambda_J = 0.13 \times (1+z)^{-3/2}(1+\delta)^{-1/2} \frac{\sigma_v}{\rm km/s} {\rm Mpc} \tag{4}$$

A rough estimate of the mass of the fragments can be calculated by assuming that the average density contrast of the filament, $\delta \approx 10$ is a slowly varying function of redshift between $z = 5$ and $z = 2$, and that typical velocity dispersions are of the order of 20 km/s$^\star$. We then get

$^\star$ This value is based on the averaged velocity dispersion of particles measured in the simulated filaments at local overdensities of around 10.

$8 \times 10^9 \mathrm{M}_\odot \leq \mathrm{M_J} \leq 2 \times 10^{10} \mathrm{M}_\odot$, to be compared to the mass functions for new haloes given in Fig. 3 (right panel) at redshifts 3.5, 2 and 1. We observe that the masses of the new WDM halo are actually close to these estimated values for the Jeans mass, thus supporting the assumption that they do indeed form through a fragmentation of the filament caused by gravitational instability. Now, the same range of values for $\delta$, $z$ and $\sigma_v$ yields 53 kpc $\leq \lambda_\mathrm{J} \leq$ 150 kpc which validates our assumption for the homogeneity of the WDM filament density field on these scales since the free–streaming length $R_f$ of a 0.5 keV particle is $R_f \simeq 300$ kpc corresponding to a free streaming mass $M_f \simeq 4 \times 10^{10} \mathrm{M}_\odot$. Note that this is not the case for the CDM filament as the free-streaming scale associated with the cold particle is much smaller than the Jeans length, and therefore we cannot consider the density field as homogeneous on these scales. Moreover, one consideration regarding the simulation technique needs to be borne in mind: our $N$-body code `MLAPM` achieves high spatial resolution primarily in high density regions. This means that the force resolution can smooth out the density field on scales above the Jeans mass in lower density regions, with the result that one would then tend to identify haloes as 'new' that should have already collapsed on smaller scales at earlier times. Nevertheless this possible numerical fragmentation is not too much of a concern in the present study, because even if one was to consider *all* the new haloes identified in the CDM filament at *all* redshifts as numerical artifacts, one still would have to invoke physical fragmentation to explain how the more massive new WDM haloes formed (see Fig. 3).

### 3.5 Merger History in Filament

Parallel to fragmentation and creation of new haloes, we also measure the rate of major mergers within the filaments in both models. A major merger event is defined by the ratio of the two most massive progenitors: if this ratio is smaller than 3:1, then the merger is major, otherwise it is minor. As before, a lower mass cut-off of $10^9 h^{-1}$ $\mathrm{M}_\odot$ is applied for each halo. Fig. 7 indicates that at early times (high redshift) there is no major merger activity in the WDM filament whereas at later times the relative fraction of major mergers exceeds that found in the CDM scenario. This supports our previous claim that haloes at high redshift ($z > 3$) do not form according to the traditional bottom-up hierarchy (i.e. via mergers) in the WDM filament. Moreover, since the mass distribution of the fragments formed through the top-down mechanism between $z = 5$ and $z = 2$ is broadly peaked around the Jeans mass (see Fig. 3), one naturally expects the major merger activity to reach a maximum around $z = 2$ in WDM because this epoch combines a high number density of low mass halos with a small mass spread in their distribution. In other words, at redshift higher than 2, quite a large fraction of small halos are still forming from fragmentation, and at lower redshift most of the formation and merging have already taken place, broadening the mass distribution function. As a result of these effects, the major merger fraction is strongly suppressed both at low and high redshifts. On the other hand, in the CDM filament, the fraction of major mergers is almost constant in time and reaches more modest values. This is the result of most of the haloes being already in place at high redshift ($z > 5$) which guarantees that the mass distribution of haloes will broaden smoothly over time as merging and accretion proceed.

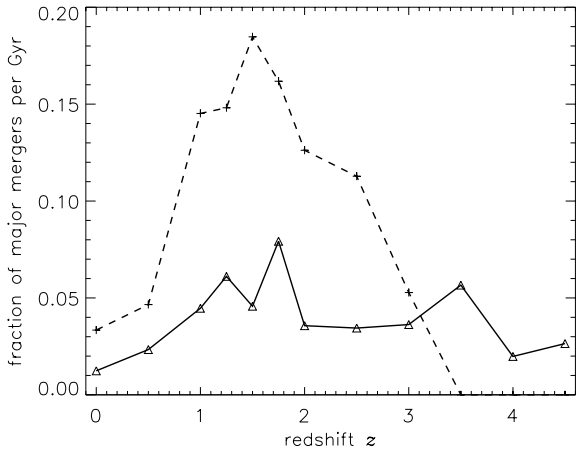


**Figure 7.** Fraction of merger events per Gyr for which the ratio of the two most massive progenitors is higher than 3:1 (major mergers).

## 4 DISCUSSION AND CONCLUSIONS

We presented the first high resolution $N$-body simulation of the top-down formation of dark matter halos through the fragmentation of a dark matter filament. This leads to a number of interesting results: the epoch of formation of small haloes is pushed back in time to lower redshifts ($2 < z < 5$) with respect to the standard CDM model, and the mass distribution of the fragments is broadly peaked around a Jeans mass of a few $10^9$ $\mathrm{M}_\odot$, corresponding to a gravitational instability of smooth regions with an overdensity contrast around 10 at these redshifts. We need to undertake detailed hydrodynamic and star formation simulations to properly assess the impact of such a mode of formation on dwarf galaxies, but we anticipate the predictions in terms of clustering and the mean age of the stellar populations to be quite different from those of the standard CDM model. We defer this study to a companion paper. Reionisation of filamentary structures might not be a problem since we have shown that massive objects are already in place at z = 5. Of course, the higher the redshift the more difficult it will be to reionise the universe unless the decrease in the number of objects is compensated by an increase in the efficiency of the ionising sources. Our numerical simulations strongly suggest that spurious numerical fragmentation may occur in CDM models due to the softening of the gravity force. However, this is not to be confused with the real fragmentation observed in the WDM simulation presented here because in AMR codes such as `MLAPM` the force resolution is a function of the mass resolution. Therefore, two haloes with the same number of particles in the ΛCDM and ΛWDM simulations are resolved with the same force resolution. This implies that if we were dominated by artificial fragmentation in both ΛCDM and ΛWDM we should not observe different upper mass cut-offs in the mass distribution functions of new halos. Looking at Fig. 3 we clearly see that

this is not the case: the mass distribution of new halos in ΛCDM drops off sharply at $\approx 2 \times 10^9 h^{-1}$ $M_\odot$ whereas it extends to masses $\gtrsim 10^{10} h^{-1}$ $M_\odot$ in ΛWDM. Furthermore, the resolution of our new WDM haloes is high enough that they should have been detected by the BDM algorithm at higher redshift had they been present at that time, since CDM haloes as massive are indeed classified as old ! Finally, we point out that Melott (1982) already showed that galactic haloes were forming via real fragmentation in Hot Dark Matter simulations where the resolution was several orders of magnitudes below what we achieve in this study. In light of these remarks, we conclude that while our results for the formation of massive (at least several hundred particles) WDM haloes through fragmentation are robust, a more detailed study is needed in order to really quantify numerical fragmentation effects on smaller scales, as they might be relevant for studies of dwarf galaxies in cosmological contexts where small haloes are not sufficiently resolved. More specifically, we believe these numerical effects will lead to a later formation of low mass haloes in moderately overdense regions.

**Acknowledgments**

The simulations presented in this paper were carried out on the Beowulf cluster at the Centre for Astrophysics & Supercomputing, Swinburne University and the Oxford Supercomputer Centre. AK acknowledges the support of the Swinburne University Research Development Grants Scheme. JEGD acknowledges enlightening discussions with James Taylor about granularity, and with Greg Bryan about numerical resolution issues. The research of JEGD at Oxford is supported by a major grant from the Leverhulme trust. BKG acknowledges the support financial support of the Australian Research Council.

## REFERENCES

Avila-Reese V., Colin P., Valenzuela O., D'Onghia E., Firmani C., 2001, ApJ, **559**, 516
Bennett C.L., et al., `astro-ph/0302207`
Benson A.J., Frenk C.S., Lacey C.G., Baugh C.M., Cole S., 2002, MNRAS, **333**, 177
Binney, J., & Tremaine, S. 1987, *Galactic Dynamics*, Princeton: Princeton University Press
Bode P., Ostriker J.P., Turok N., 2001, ApJ, **556**, 93
Chen J., Kravtsov A.V., Keeton C.R., 2003, ApJ, **592**, 24
Colin P., Avila-Reese V., Valenzuela O., 2000, ApJ, **542**, 622
Dalal N., Kochanek C.S., 2002, ApJ, **572**, 25
Einasto J., Einasto M., Tago E., Mueller V., Knebe A., Cen R., Starobinsky A. and Atrio-Barandela F., 1999, ApJ, **519**, 456

de Blok W. J. G., Bosma A., 2002, A&A, **385**, 816
Kamionkowski M., Liddle A.R., 2000, Phys. Rev. Lett., **84**, 4525
Kaplinghat M., Knox L., Turner M.S., 2000, Phys. Rev. Lett., **85**, 3335
Klypin A.A., Holtzman J., `astro-ph/9712217`
Knebe A., Green A., Binney J., 2001, MNRAS, **325**, 845
Knebe A., Devriendt J.E.G., Mahmood A., Silk J., (paperI) 2002, MNRAS, **329**, 813
Kogut A., et al. `astro-ph/0302213`
Little B., Knebe A., Islam R.R., 2003, MNRAS, **341**, 617
Kravtsov A.V., Klypin A.A., Khokhlov A.M., 1997, ApJ, **111**, 73
Melott A.L., 1982, MNRAS, **296**, 721
Metcalf R.B., Madau P., 2001, ApJ, **563**, 9
Power C., Navarro J.F., Jenkins A., Frenk C.S., White S.D.M., Springel V., Stadel J., Quinn T., 2003, MNRAS, **338**, 14
Schneider R., Ferrara A., Natarajan P., Omukai K., 2002, ApJ, **571**, 30
Somerville R.S., 2002, ApJ Lett., **572**, 23
Spergel D.N., Steinhardt P.J., 2000, Phys. Rev. Lett., **84**, 3760
Spergel D.N., et al. `astro-ph/0302209`
Swaters R. A., Madore B. F., van den Bosch F. C., Balcells M., 2003, ApJ, **583**, 732